Antarctic atmospheric boundary layer observations with the Small Unmanned Meteorological Observer (SUMO)

John J. Cassano[1,2], Melissa A. Nigro[2], Mark W. Seefeldt[1], Marwan Katurji[3], Kelly Guinn[1,2], Guy Williams[4], Alice DuVivier[5]

[1] Cooperative Institute for Research in Environmental Sciences, University of Colorado, Boulder, CO, USA

[2] Department of Atmospheric and Oceanic Sciences, University of Colorado, Boulder, CO, USA

[3] Department of Geography, University of Canterbury, Christchurch, New Zealand

[4] Autonomous Maritime Systems Laboratory, University of Tasmania, Launceston, Australia

[5] National Center for Atmospheric Research, Boulder, CO, USA

Correspondence to: John J. Cassano (john.cassano@colorado.edu)

Abstract

Between January 2012 and June 2017 a small unmanned aerial system (sUAS), known as the Small Unmanned Meteorological Observer (SUMO), was used to observe the state of the atmospheric boundary layer in the Antarctic. During 6 Antarctic field campaigns 116 SUMO flights were completed. These flights took place during all seasons over both permanent ice and ice free locations on the Antarctic continent and over sea ice in the western Ross Sea. Sampling was completed during spiral ascent and descent flight paths that observed the temperature, humidity, pressure and wind up to 1000 m above ground level and sampled the entire depth of the atmospheric boundary layer as well as portions of the free atmosphere above the boundary layer. A wide variety of boundary layer states were observed including very shallow, strongly stable conditions during the Antarctic winter and deep, convective conditions over ice free locations in the summer. The Antarctic atmospheric boundary layer data collected by the SUMO sUAS, described in this paper, can be retrieved from the United States Antarctic Program Data Center (https://www.usap-dc.org). The data for all flights conducted on the continent are available at https://www.usap-dc.org/view/dataset/601054 (Cassano 2017; https://doi.org/10.15784/601054) and data from the Ross Sea flights, are available at https://www.usap-dc.org/view/dataset/601191 (Cassano 2019; https://doi.org/10.15784/601191).

1. Introduction

The turbulent lower portion of the atmosphere, known as the atmospheric boundary layer, is the part of the atmosphere that interacts directly with the underlying surface. In lower and middle latitudes atmospheric properties in the boundary layer change diurnally in response to the diurnal cycle of net radiation at the surface. During the day downwelling shortwave radiation often results in a positive surface radiation budget, surface heating, and the development of a convective boundary layer with temperature decreasing with height at a rate of approximately 10 K km^{-1}. At night, longwave radiative cooling from the surface results in surface cooling and the development of a statically stable boundary, often characterized by a surface based inversion, where temperature increases with height. The presence of clouds or changes in large-scale winds will alter this typical diurnal boundary layer evolution (Stull 1988).

In the polar regions a weaker, or absent, diurnal cycle in radiative forcing results in a less pronounced diurnal cycle in boundary layer evolution compared to that observed in lower latitudes, although some locations, such as the McMurdo Dry Valleys, do experience a pronounced diurnal cycle during the austral summer (Katurji et al. 2013). The presence of extensive ice covered surfaces reduces the amount of solar radiation absorbed at the surface during the day and weakens, or eliminates, the presence of convective boundary layer conditions. During the long polar night extended periods of radiative cooling at the surface lead to the development of stably stratified boundary layers with strong temperature inversions, although strong winds or clouds can cause the surface inversion to dissipate and well mixed conditions to develop (King and Turner 1997; Cassano et al. 2016a; Nigro et al. 2017).
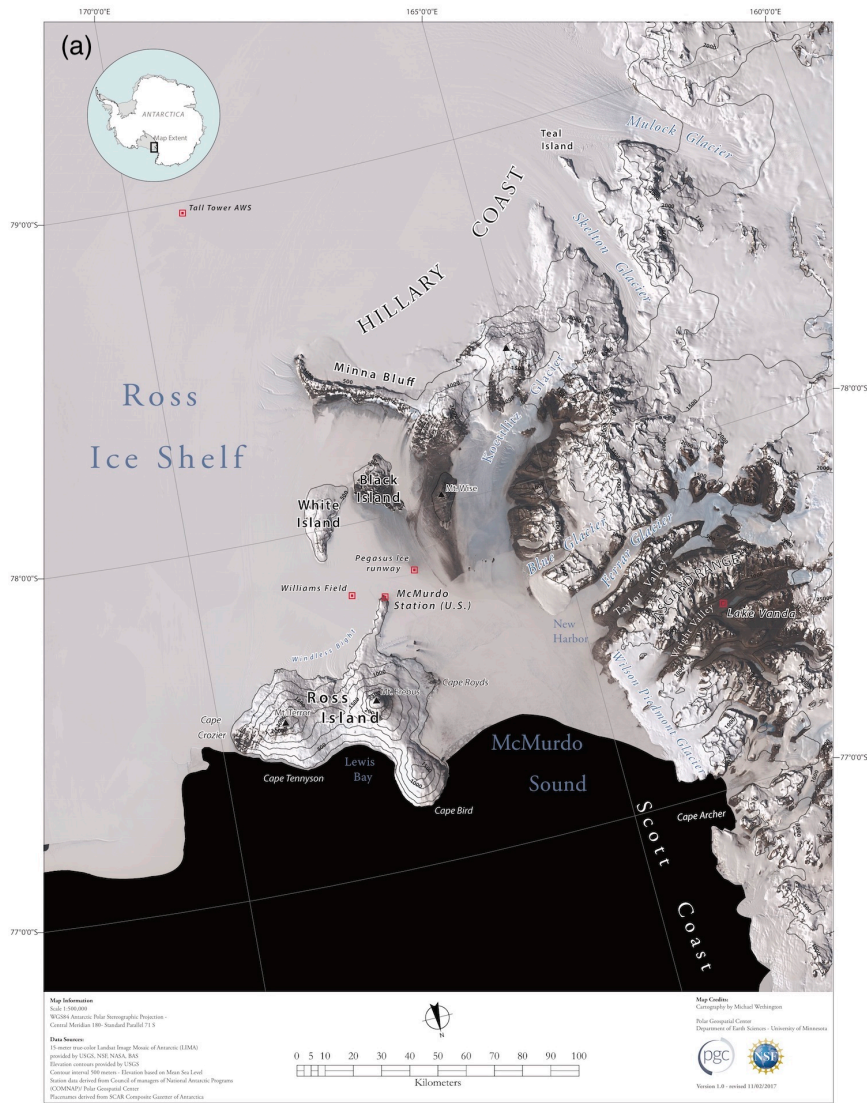
The vast majority of in-situ atmospheric observations in the Antarctic are surface observations within the lowest 10 m of the atmosphere with very few observations made above the surface (Summerhayes 2008). This lack of information on the vertical structure of the atmosphere, even in the lowest 10s to 100s of meters, limits our ability to study the Antarctic boundary layer. Cassano et al. (2016a) provide a summary of Antarctic boundary layer studies that made in-situ observations of vertical profiles of atmospheric properties. Antarctic field campaigns from the 1950s

to present have often relied on data collected on meteorological towers that extend up to 50 m

65 above the surface.

More recently several groups have used unmanned aerial systems (UAS) to observe the Antarctic boundary layer (Cassano 2014). The British Antarctic Survey was the first to use UAS for Antarctic boundary layer observations with 20 science flights conducted in October and December 2007 (P. Anderson, personal communication 2013). Cassano et al. (2010, 2016b) and Knuth et al.

70 (2013) describe UAS flights which observed air-sea exchanges in the Terra Nova Bay polynya in the western Ross Sea. The Finnish Meteorological Institute has conducted UAS flights in Dronning Maud Land, Antarctica, at the Aboa research station. Several different UAS were deployed from the *RV Polarstern* ice breaker in the Weddell Sea during the austral winter of 2013 (Jonassen et al. 2015).

75 Our research group has used an easily deployed small UAS (sUAS) known as the Small Unmanned Meteorological Observer (SUMO) (Reuder et al. 2009) during six Antarctic field campaigns from 2012 through 2017. These SUMO campaigns have occurred on the Ross Ice Shelf, near Ross Island, and in the McMurdo Dry Valleys (Fig. 1) in the austral summer and late austral winter into early spring. Austral autumn and winter SUMO flights were conducted as part of

80 the polynyas, ice production and seasonal evolution in the Ross Sea (PIPERS) research cruise in the western Ross Sea from April to June 2017 (Ackley et al. 2020). The SUMO campaigns were conducted over permanent ice shelves in areas with little topography within 100 or more km as well as in regions of very complex terrain with elevations rising over 4000 m within 30 km of the flight locations. Other flights occurred over the ice free, complex terrain of the Wright Valley and over the

85 sea ice of the Ross Sea. The data collected over these varied surfaces over the entire annual cycle provides observations of a wide range of Antarctic boundary layer conditions.
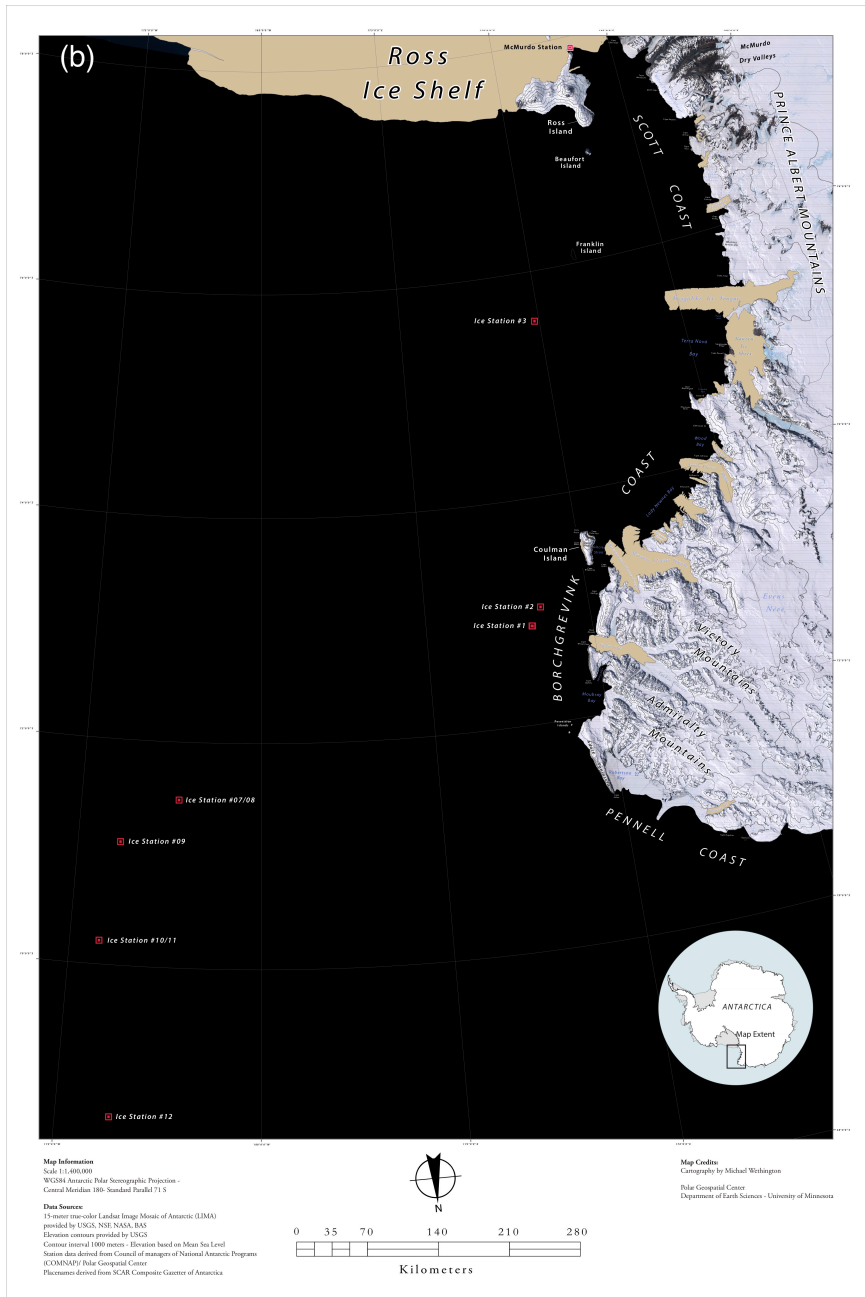
Deleted: ,

Deleted: easily deployed

4

(a)

ANTARCTICA
Map Extent

Tall Tower AWS

170°0'0"E
165°0'0"E
160°0'0"E

79°0'0"S

HILLARY COAST

Mulock Glacier

Teal Island

Skelton Glacier

Ross Ice Shelf

Minna Bluff

78°0'0"S

Koettlitz Glacier

White Island

Black Island

Mt. Wace

Blue Glacier

Ferrar Glacier

Taylor Valley

ASGARD RANGE

Lake Vanda

Wright Valley

Pegasus Ice runway

Williams Field

McMurdo Station (U.S.)

New Harbor

Weldon Piedmont Glacier

Cape Royds

Mt. Erebus

Ross Island

Cape Crozier

Mt. Terror

McMurdo Sound

77°0'0"S

Cape Tennyson

Lewis Bay

Cape Bird

Cape Archer

Scott Coast

77°0'0"S

Map Information
Scale 1:500,000
WGS84 Antarctic Polar Stereographic Projection -
Central Meridian 180- Standard Parallel 71 S

Data Sources:
15-meter true-color Landsat Image Mosaic of Antarctica (LIMA)
provided by USGS, NSF, NASA, BAS
Elevation contours provided by USGS
Contour interval 500 meters - Elevation based on Mean Sea Level
Station data derived from Council of managers of National Antarctic Programs
(COMNAP)/ Polar Geospatial Center
Placenames derived from SCAR Composite Gazetteer of Antarctica

N

0 5 10   20   30   40   50   60   70   80   90   100
Kilometers

Map Credits:
Cartography by Michael Wethington

Polar Geospatial Center
Department of Earth Sciences - University of Minnesota

pgc   NSF

Version 1.0 - revised 11/02/2017

90

5

(b)

Ross
Ice Shelf

McMurdo Station

McMurdo
Dry Valleys

Ross
Island

Beaufort
Island

Franklin
Island

SCOTT COAST

PRINCE ALBERT MOUNTAINS

Ice Station #3

Terra Nova
Bay

Wood Bay

COAST

Coulman
Island

BORCHGREVINK

Ice Station #2

Ice Station #1

Victory
Mountains

Admiralty
Mountains

Ice Station #07/08

PENNELL COAST

Ice Station #09

Ice Station #10/11

ANTARCTICA

Map Extent

Ice Station #12

N

| 0 | 35 | 70 | 140 | 210 | 280 |

Kilometers

6

Figure 1: Location of all SUMO sUAS boundary layer flights (red squares) over the Antarctic continent (a) and the Ross Sea (b). Maps prepared by Michael Wethington, Polar Geospatial Center, Department of Earth Sciences, University of Minnesota.

This paper describes the SUMO sUAS and flight strategy employed during our Antarctic field campaigns (section 2), the data processing and quality control applied to the data (section 3), provides examples of boundary layer features that were observed with the SUMO sUAS (section 4) and the SUMO data availability (section 5). A brief summary is presented in section 6.

2. The SUMO sUAS and flight strategy

2.1 SUMO sUAS

Reuder et al. (2009; 2012), Cassano (2014), and Jonassen et al. (2015) provide technical descriptions of the SUMO sUAS. The SUMO is a small fixed wing pusher prop drone with 0.80 m wingspan and 580 g take-off weight that is constructed from high-density foam (Fig. 2). The airframe is based on the commercially available Multiplex Funjet model remote control airplane. The SUMO uses a single lithium polymer (LiPo) battery to power the electric motor, which allows for a flight time of ~30 minutes. Further details about the SUMO sUAS are given in Table 1.

Figure 2: SUMO sUAS at the Pegasus ice runway outside of McMurdo Station, Antarctica.

115   Table 1: SUMO sUAS airframe and flight specifications (after Reuder et al. 2012 and Cassano 2014).

Wingspan	0.80 m
Length	0.75 m
Propeller diameter	227 mm
Take-off weight	580 g
Motor	120 W electric brushless
Battery	2.1 Ah, 11.1 V lithium polymer
Speed (min / cruise / max)	8 m s^{-1} / 15 m s^{-1} / 25 m s^{-1}

8

Horizontal range	5 km
Vertical range	4 km a.g.l.
Flight duration	~30 min

120   The SUMO sUAS is launched by hand and lands on its underside. Usually a two-person team operates the SUMO. One person, the remote control pilot, maintains visual sight of the aircraft and controls the SUMO via a remote control while the second flight team member, the ground station pilot, manages the ground control software. A standard model airplane remote control can be used to manually control the SUMO sUAS but it is typically flown in a semi-autonomous or

125   autonomous mode via the onboard Paparazzi autopilot (ENAC 2008) and ground control software (Table 2). A 2.4 GHz radio modem is used for two-way communication between the SUMO and the ground control software. The SUMO observations are relayed to the ground station computer and the pre-programmed flight plan can be modified with the ground station software via the radio modem link. In case of a ground station communication failure the remote control pilot can take

130   control of the aircraft at any time.

Table 2: SUMO sUAS navigation, control and communication and scientific instrumentation sensor range, accuracy, acquisition frequency and time constant, as specified by the manufacturer (after Reuder et al. 2012 and Cassano 2014).

135

Navigation, Control and Communication					
Auto-pilot navigation	On-board GPS				
Manual navigation	Model airplane remote control				
Attitude control	Diydrones Ardu inertial measurement unit (IMU)				
Communication	2.4 GHz two-way data link with Toughbook laptop computer				
Scientific Instrumentation					
Meteorological Parameter	Sensor	Range	Accuracy	Acquisition Frequency	Sensor Time

					Constant
Pressure	VTI SCP1000	300-1200 hPa	0.5 hPa relative accuracy	4 Hz	Not available
Temperature	Pt 1000 Heraeus M222	-32 to 96°C	±0.2 K	8 Hz	~3 s
Temperature	Sensirion SHT 75	-40 to 124°C	±0.3 K	2 Hz	5 to 30 s
Humidity	Sensirion SHT 75	0-100%	±2%	2 Hz	~8 s
Wind	"No flow sensor" algorithm (Mayer et al. 2012)	Not applicable	Wind speed: ~1 m s^{-1} Wind direction: ~5°	~30 s	Not applicable

The SUMO records temperature, humidity, pressure and aircraft location at 2 to 8 Hz frequency (Table 2). Temperature is measured with a reported accuracy of ± 0.2 K (± 0.3 K) for the

140 Pt 1000 (Sensirion) sensor. The temperature sensor specifications indicate a time lag of 3 to 30 s but comparison between the two temperature sensors indicate that both have a similar lag of 2 to 5 s. The sensor lag appears as an offset between ascending and descending temperature profiles during flights with continuous spiral ascent and descent flight patterns as shown in Cassano (2014) and discussed in Section 4. As a result of this sensor lag most of the SUMO flights described in

145 this paper used stepped ascent or descent profiles (described in more detail below). Each step in these ascent / descent patterns occurred over roughly 65 s so the temperature sensor lag becomes unimportant as it is much shorter than the orbit time at each height. The reported sensor time constant for relative humidity measurements, made with the Sensirion SHT 75 sensor, is approximately 8 s although at temperatures well below 0ºC we found that the humidity data was

150 largely unusable due to very long time lags. The Mayer et al. (2012) "no flow sensor" method was used to estimate wind speed and direction by evaluating differences in ground speed throughout a circular flight path and is described in greater detail in section 3.

2.2 Flight Strategy

A total of 116 SUMO sUAS flights took place between January 2012 and June 2017 at several locations in Antarctica (Fig. 1). Many of these flights took place over permanent ice shelf locations with 8 flights at Williams Field, 39 flights at the Pegasus ice runway and 36 flights at the Tall Tower AWS site (Wille et al. 2017). Pegasus runway and Williams Field are within 20 km of the main United States Antarctic Program research base, McMurdo Station, and Ross Island, which has a maximum elevation in excess of 4000 m. The Tall Tower AWS flights took place approximately 160 km south southeast of McMurdo Station in a region of almost completely flat permanent ice with no major topographic features within 85 km of the site. Other continental flights occurred near Lake Vanda in the ice free McMurdo Dry Valleys (14 flights). Finally, several flights occurred over sea ice in the western Ross Sea as part of the PIPERS cruise (19 flights; Ackley et al. 2020). To avoid issues related with aircraft icing all flights occurred in cloud free conditions, over the altitude range of the flight, although clouds above the maximum flight level were present for some flights. Table A1 lists the date and time, location and maximum altitude for each flight.

Additional Antarctic SUMO flights had been planned to take place after the PIPERS cruise in 2017, but challenges in attempting to schedule a mid-winter campaign as well as the recent Antarctic field work restrictions due to COVID-19, resulted in the 2017 flights being the last SUMO flights conducted in Antarctica. As such, this paper provides a description of all Antarctic SUMO UAS flights that have been, or will be, conducted by our research group. Future sUAS flights in Antarctica, led by our group, will use the DataHawk2 sUAS, developed at the University of Colorado - Boulder (Lawrence and Balsley 2013).

The primary scientific objective for all of our Antarctic SUMO flights was to obtain profiles of the atmospheric state of the boundary layer. During a given flight day SUMO boundary layer profile flights would occur every hour to several hours, although other factors, including weather and logistics, could limit the frequency and number of flights that could be performed. Changes in the atmospheric thermodynamic state between pairs of SUMO profile flights allowed for estimation of the surface turbulent fluxes, based on state changes within the boundary (Bonin et al. 2013; Båserud et al. 2020), as well as estimates of large-scale advective changes, based on state

11

changes above the boundary layer. The relatively high temporal resolution atmospheric profiles observed by the SUMO were also used to assess Antarctic Mesoscale Prediction System (Powers et al. 2012) operational weather forecasts (Wille et al. 2017).

A typical flight started with the SUMO manually or semi-autonomously controlled by the remote control pilot. Immediately after launch the remote control pilot would ensure that the SUMO sUAS was performing as expected and would then switch the aircraft to the fully autonomous flight mode. The aircraft would then climb to a specified height (usually 50 m agl) and orbit until instructed, by the ground control pilot via the ground control software, to begin the profiling portion of the flight. A stepped spiral ascent / descent flight pattern was usually used with the aircraft set to orbit at several different heights below a maximum altitude of 1000 m agl. For most flights a stepped ascent was followed by a continuous descent, although some flights had a stepped ascent followed by a stepped descent. A few flights were also flown with a continuous spiral ascent followed by a continuous spiral descent, although as discussed above this flight pattern resulted in noticeable artifacts due to sensor lag. For both the stepped and continuous profiles the spiral diameter was approximately 250 m. The SUMO would complete two circular orbits, in approximately 65 s, at each specified height in the stepped ascent / descent profile before climbing or descending to the next fixed height orbit location. Once the profiling was completed the aircraft would return to a height of approximately 50 m and orbit until the remote control pilot took control of the aircraft to land it in either manual or semi-autonomous mode.

The boundary layer depth in the Antarctic can vary from 10s of m or less during strongly stable, light wind conditions in winter to more than 1000 m in summer (King and Turner 1997). The maximum SUMO spiral profile heights ranged from 89 m to 1371 m agl (Table A1) and sampled the full depth of the boundary layer for all but a few flights. The continuous spiral ascent and descent flight pattern, up to 1000 m agl, usually took about 10 min to complete and two to three profiles could be completed in a single flight. For the stepped ascent or descent profile flight patterns it was usually possible to complete 18 fixed height orbits during a 30 minute flight.

3. Data processing and quality control

12

Deleted: Some flights were conducted with

215   Data from the SUMO sUAS were logged using an onboard datalogger controlled through the Paparazzi autopilot software. This data was telemetered, via 2.4 GHz radio modem, to a laptop computer running the Paparazzi ground control software and also logged to an onboard SD memory card. The data in the telemetered and SD data streams were identical, other than a reduced temporal resolution and occasional gaps in the record in the telemetered data. The SD

220   data stream was used as the source data for the archived data except for cases where the SD data was not available due to memory card failure or other issues.

        The data recorded by the SUMO, in both the telemetered and SD data stream, is written sequentially with each record marked with the elapsed time since the SUMO was powered on. Each data record reported a single variable – aircraft status, navigation information or data from

225   one of the scientific instruments. This data was stored in text log files on the ground station computer and the onboard SD card.

        Following each flight the SUMO SD, or telemetered, log files were processed into a comma separated text file. A header was written to this file that listed the flight location, sUAS pilots and start date and time of the flight. Each subsequent line of the file listed the date and time, elapsed

230   time since SUMO power on, location and meteorological data (Table A2) at the same temporal frequency as the original SUMO data file. The date and time variables were calculated from the date and time on the ground station laptop when the SUMO was powered on and the elapsed time reported for each record in the data file. Since each time period reported in the SUMO data file listed a single variable all other variables were flagged as missing values (-9999) for that time

235   period. These data files were named yy_mm_dd__HH_MM_SS_SD.txt, where yy is year, mm is month, dd is day, HH is hour, MM is minute and SS is second of the SUMO power on time in UTC. The _SD indicates that the data is from an SD file. If the data came from a telemetered SUMO log file the _SD was omitted in the filename.

        A second data processing step linearly interpolated all variables in time to replace the

240   missing data values and provide data for all variables at each time step in the data file. No interpolation was performed before a given variable was first reported in the log file so these records retain missing data values. This data was written to files with the same naming convention as above
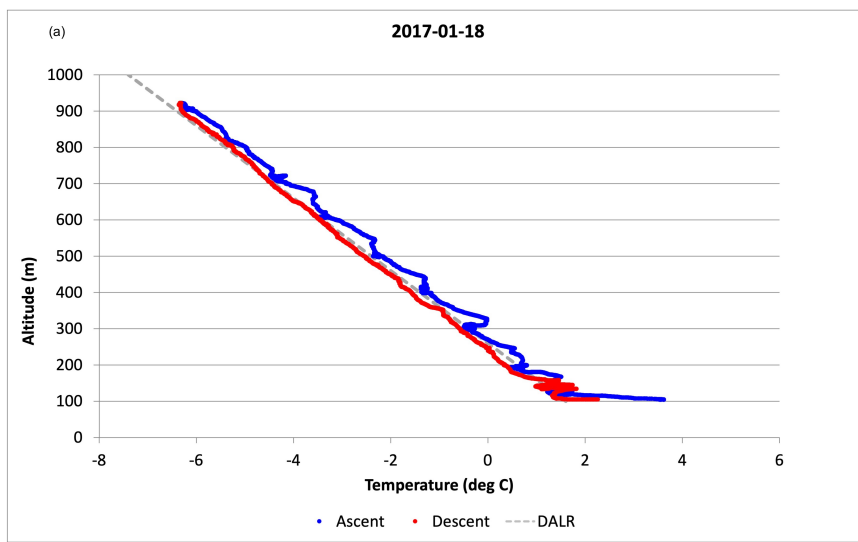
but with _interpolation added to the filename before the .txt filename extension to indicate the temporal interpolation was applied to the original data.
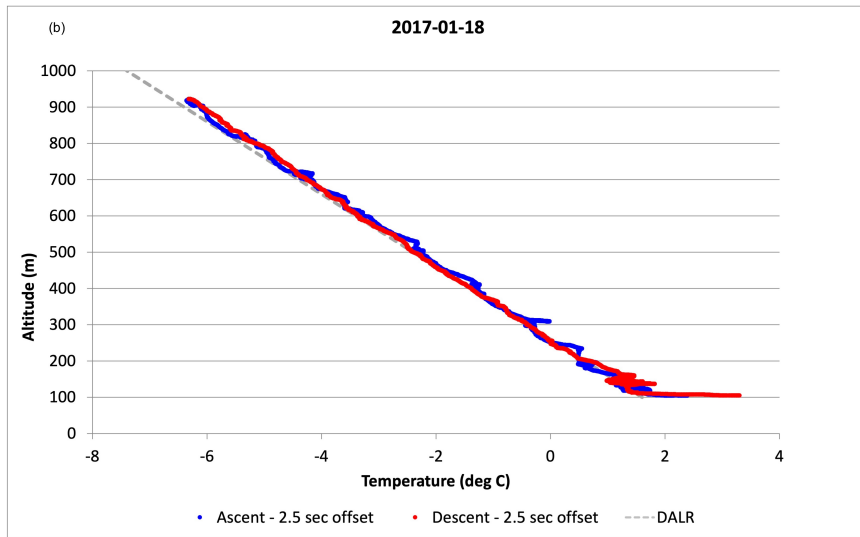
245   The interpolated data was then used to calculate averages from each constant altitude orbit completed during the flight and vertical bin averages. As described above, most SUMO flights were conducted such that the sUAS orbited at multiple fixed heights over the flight altitude range. These fixed height orbits helped address sensor time lag issues and also allowed the Mayer et al. (2012) "no flow sensor" algorithm to estimate winds at a constant altitude. This processing step

250   identified flight segments that remain within ±8 m of all other points in the segment and for all segments when the SUMO's position on the circular orbit passed through a full 360° (i.e. one complete circular orbit). For each flight segment identified in this way the wind speed and direction was estimated following Mayer et al. (2012) and the average altitude, temperature, relative humidity and pressure was calculated. The wind speed was estimated based on the difference between the

255   minimum and maximum GPS ground speed recorded during the circular orbit. The wind direction was calculated based on the orbit heading at the location of the minimum and maximum GPS speed, with both directions reported in the archived data file. The start and end time, heading and altitude, as well as elapsed time, on the constant height orbit were also reported in the archived data file named yy_mm_dd_HH_MM_SS_SD_const_alt.txt. All data stored in the constant altitude

260   archived data file are listed in Table A2.

Vertical bin averages were calculated for each 5 m altitude bin over the full altitude range of each SUMO flight. For each vertical altitude bin the average, standard deviation and number of observations in the bin was calculated. These values were calculated from all data during the flight as well as from data from the ascent-only and descent-only portions of the flight. This data is stored

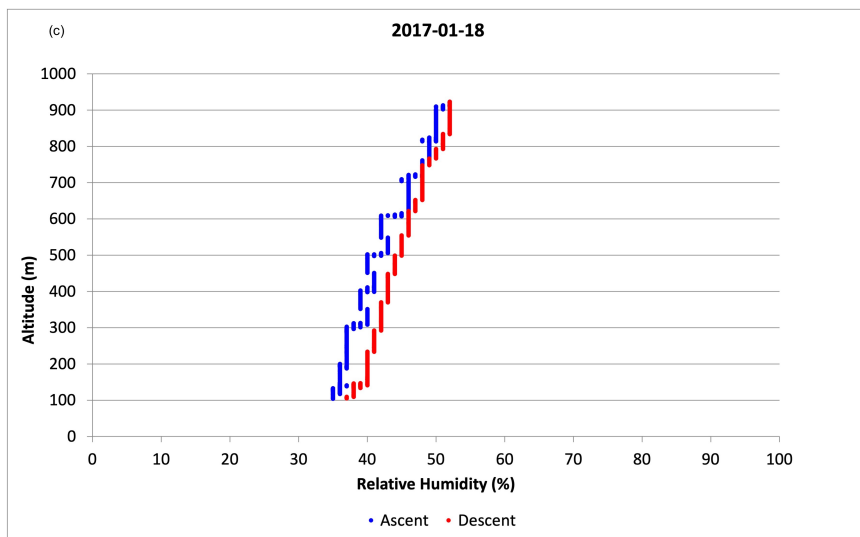265   in files named yy_mm_dd__HH_MM_SS_SD_vert_avg.txt (Table A2).

Data from each flight, in the interpolated data file as well as from the vertical bin average and constant altitude orbit data files was visually inspected. The following issues were observed, but no data was removed from the archived data files. For each flight, there is a short period, of a few seconds, when the temperature sensors adjust to the ambient conditions immediately after

270   take-off. As noted in section 2.1 there is a noticeable sensor lag evident in the temperature and
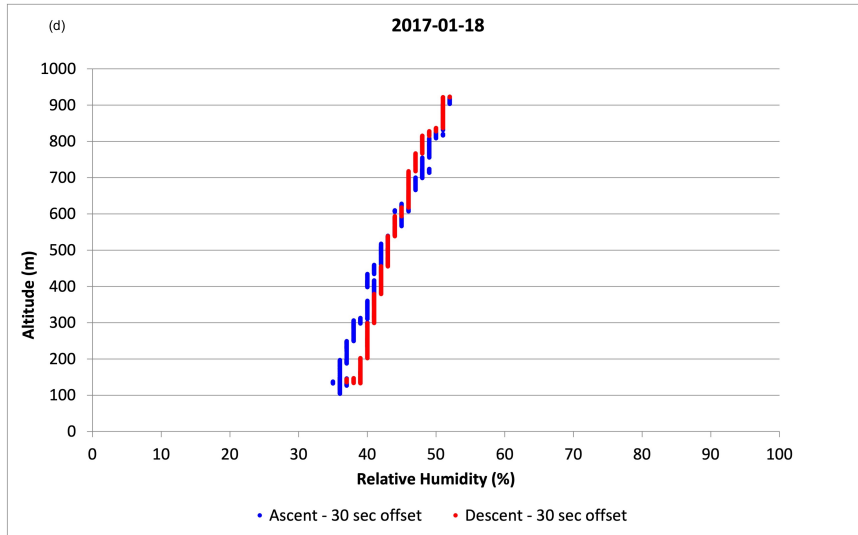
14

humidity measurements. The sensor lag is short, of the order of a few seconds, for the temperature measurements but is much longer for the humidity observations. These lags are obvious when comparing observations from the ascent and descent portions of the flight (Fig. 3). Since the original time resolution data is provided users of this data can apply whatever corrections are needed for their application to account for the sensor lag, but no corrections were applied to the archived data.

(a)

2017-01-18

2017-01-18

(b)

Altitude (m) vs Temperature (deg C)

- Ascent - 2.5 sec offset
- Descent - 2.5 sec offset
- DALR

280

2017-01-18

(c)

Altitude (m) vs Relative Humidity (%)

- Ascent
- Descent

Figure 3. Temperature (a and b) and relative humidity (c and d) profiles observed by the SUMO sUAS in the Wright Valley, Antarctica at 0201 UTC 18 January 2017. The original time interpolated data is plotted in panels a and c and data with a time lag of 2.5 s and 30 s is plotted in panels b and d, respectively. In panels (a) and (b) the dry adiabatic lapse rate (DALR) is shown with a gray dashed line.

Figure 3 illustrates the sensor lag for temperature and humidity measurements for a SUMO flight conducted at 0201 UTC 18 January 2017 in the Wright Valley. During this flight a deep, convective boundary layer was present. Figure 3a shows the temperature observed during the stepped ascent (blue) and spiral descent (red) portions of this flight. The ascent portion of the flight is consistently warmer than the descent and given the decreasing temperature with height on this day, is consistent with a short time lag in the temperature measured by the SHT sensor. By applying a 2.5 s offset to the temperature, relative to the height, the ascent and descent profiles more closely match (Fig. 3b). This time lag is consistent with results presented by Cassano (2014). The humidity observations also exhibit a time lag (Fig. 3c). Here, humidity increases with height and the time lag

17

300   results in the ascending observations being shifted to slightly lower relative humidity values, at a

given height, compared to the observations during the descent. While the manufacturer stated

sensor time constant for the humidity sensor is ~8 s, we have found that applying a 30 s time shift

to the humidity measurements results in much closer correspondence between the humidity profiles

observed during the SUMO ascent and descent (Fig. 3d), although this does not fully remove the

305   discrepancies between the ascent and descent profiles as seen for temperature (Fig. 3b). The

longer time constant for the humidity measurements presented here, compared to the

manufacturer's specification, may be caused by a lower ambient temperature during these flights

than used by the manufacturer.

310   **4. Examples of Observed Features**

With SUMO flights being conducted throughout the full annual cycle and over a variety of

surface conditions across the Antarctic continent a wide range of boundary layer stability, depth

and evolution have been observed. Some examples of the variety of boundary layer states

observed by the SUMO UAS are given below.

315   Eleven SUMO flights were conducted at the Ross Ice Shelf Tall Tower site over a 14.5 h

period from 1916 UTC 20 January 2014 to 0944 UTC 21 January 2014 (Fig. 4). The timing between

most of these flights was ~1.5 hours which provided a detailed depiction of the temporal evolution

of the boundary layer and free atmosphere above.

From 1916 UTC 20 January to 0204 UTC 21 January a shallow, well mixed boundary was

320   observed, with a dry adiabatic temperature profile up to a maximum height of 250 m. After 0204

UTC the boundary layer transitioned to a weakly stable temperature profile. The temperature in the

boundary layer initially cooled (1916 to 2144 UTC 20 January) ~1 K and then warmed ~5 K by 0731

UTC 21 January before cooling ~2 K over the next approximately 2 hours.
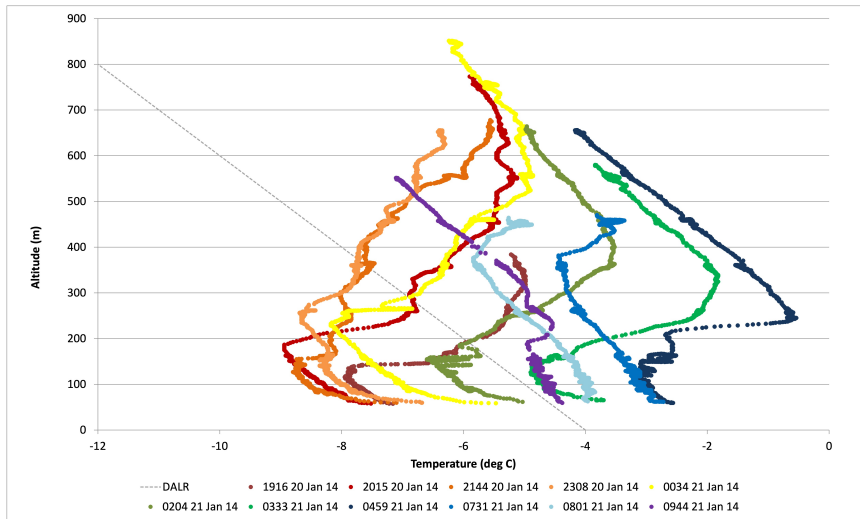
Deleted: A

Figure 4: SUMO observed temperature profiles (plotted as colored lines) at the Ross Ice Shelf Tall Tower AWS site from 1916 UTC 20 January 2014 to 0944 UTC 21 January 2014. The dry adiabatic lapse rate (DALR) is shown with a gray dashed line.

The temperature above the boundary layer was not constant during the 14.5 h sampling period from 20-21 January 2014. Here, we assume that the temperature change observed above the boundary layer is due to large-scale advective changes, but other processes such as adiabatic changes due to vertical motion or radiative heating or cooling may also contribute to the observed temperature trends. Further analysis would be required to determine the relative role of each of these processes in altering the temperature aloft. Considering the temperature at 300 m, the temperature cooled ~3 K from 1916 to 2308 UTC 20 January. This cooling was greater than what was observed in the boundary layer during this same time period and suggests that large-scale advective cooling, as inferred from the cooling aloft, was offset by an upward sensible heat flux in the boundary layer, consistent with the convective conditions observed at this time. Over the next four flights (0034 to 0459 UTC 21 January) the temperature at 300 m warmed almost 8 K, while the boundary layer temperature did not warm as much. This suggests that large-scale warm

19

advection occurring at this time was offset by either radiative cooling or a downward sensible heat flux in the boundary layer, consistent with the transition from a convective to slightly stable boundary layer during this time period. During the final three flights (0731 to 0944 UTC 21 January) cooling of ~1 K was observed aloft and in the boundary layer.

Contrasting the summer conditions seen in Fig. 4, Fig. 5 shows temperature profiles observed during 11-12 September 2016 at the Pegasus runway at the end of the Antarctic winter. Six SUMO flights were completed between 1426 UTC 11 September and 1658 UTC 12 September 2016. The surface temperature during these flights was near -40°C, which is the lower observation limit of the SHT temperature sensor. Unlike the temperature profiles shown in Fig. 4, the temperature profiles observed during the 24+ hour period from 11-12 September 2016 (Fig. 5) showed a remarkable lack of temporal variability, exhibiting nearly steady state conditions. During this time a very strong, shallow surface inversion was present with the temperature warming ~7 K in the lowest 50 m of the sounding and then warming another several K up to 200 m.
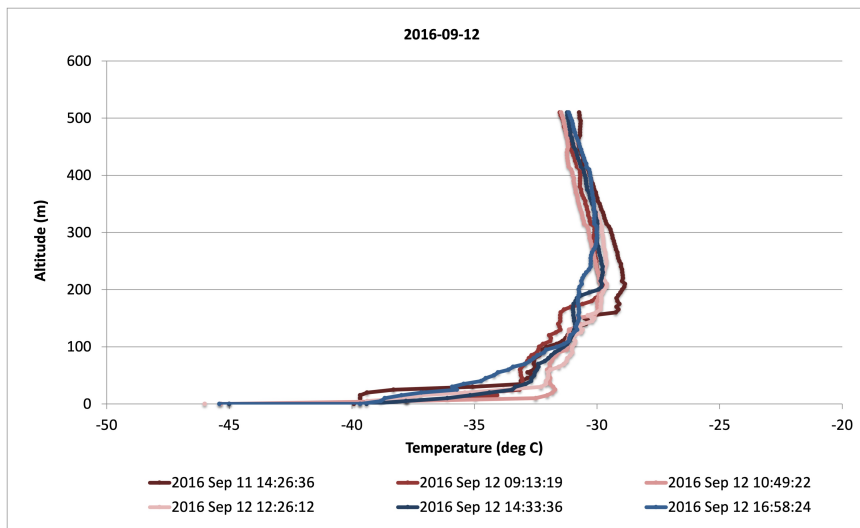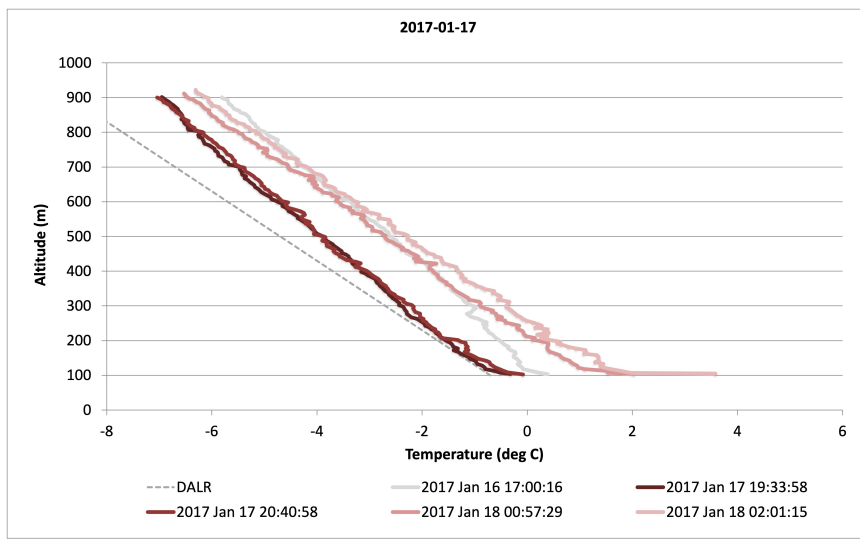

Figure 5: SUMO observed temperature profiles (colored lines) at the Pegasus Ice Runway from 1426 UTC 11 September 2016 to 1658 UTC 12 September 2016.

During the austral summer of 2017 SUMO flights were conducted in the Wright Valley, near Lake Vanda, at one of the few permanently ice free locations on the Antarctic continent. The temperature profiles observed from 16-18 January 2017 (Fig. 6) differ markedly from the profiles shown in Figs. 4 and 5. The boundary layer observed in the Wright Valley was a deep convective boundary layer with a surface temperature near or just above 0°C. From late morning to mid-afternoon local time (1933 UTC 17 Jan 2017 to 0201 UTC 18 Jan 2017) the boundary layer warmed ~2 K and deepened from 200 m to more than 800 m, with a dry adiabatic lapse rate extending beyond the top flight altitude of the SUMO at 0057 and 0201 UTC 18 January 2017.

Figure 6: SUMO observed temperature profiles (colored lines) near Lake Vanda in the Wright Valley from 1700 UTC 16 January 2017 to 0201 UTC 18 January 2017. The dry adiabatic lapse rate (DALR) is shown with a gray dashed line.

Deleted: Temperature profiles are plotted as colored lines (16 Jan 1700 UTC – gray, 17 Jan 1933 UTC – dark red; 17 Jan 2041 UTC – red; 18 Jan 0057 UTC – pink; 18 Jan 0201 UTC – light pink).

5. Data Availability

395   The SUMO sUAS data described in this paper can be retrieved from the United States Antarctic Program Data Center (https://www.usap-dc.org). The data for all flights conducted on the continent (Williams Field, Pegasus runway, Tall Tower AWS site and Wright Valley) are available at https://www.usap-dc.org/view/dataset/601054 (Cassano 2017; https://doi.org/10.15784/601054) and data from the PIPERS cruise, in the Ross Sea, are available at https://www.usap-

400   dc.org/view/dataset/601191 (Cassano 2019; https://doi.org/10.15784/601191). The data is archived in annual zip files that contain comma delimited text files of the data at its original and interpolated time resolution and as vertical bin averaged and constant altitude data. Each data file contains a header that lists the flight location name, latitude, longitude, start date and time (UTC) of the flight and the sUAS pilots. A final header line lists the data type and units contained in each

405   comma separated column in the remainder of the file.

6. Summary

        Between January 2012 and June 2017 a small unmanned aerial system (UAS), known as the Small Unmanned Meteorological Observer (SUMO), was used to observe the temperature,

410   humidity, pressure and wind in and above the Antarctic atmospheric boundary layer. During 6 Antarctic field campaigns 116 SUMO flights were completed. Flights over ice shelf locations occurred at Williams Field and the Pegasus runway (2 field campaigns), both located within 20 km of McMurdo Station and Ross Island, and at the Tall Tower AWS site located in the northwestern portion of the Ross Ice Shelf (Fig. 1). Flights also took place in the ice free Wright Valley, near Lake

415   Vanda in a region of complex terrain and were performed over sea ice, in the western Ross Sea, as part of the PIPERS research cruise (Ackley et al. 2020). These flights took place during all seasons with most of the flights conducted during the austral summer (January) and late winter / early spring (September). The flights observed the full depth of the atmospheric boundary layer and a portion of the free atmosphere above, with the SUMO flying a spiral ascent and descent flight

420   path. A wide variety of boundary layer states were observed including very shallow, strongly stable conditions during the Antarctic winter (Fig. 5) and deep, convective conditions over ice free locations in the summer (Fig. 6).

22

Data from these flights was processed from the native SUMO log files into comma separated text files at the original and an interpolated time resolution. Additional data processing, of the interpolated time resolution data, created vertical bin averaged data and averages over constant altitude SUMO orbits. Errors noted in the data include short periods of time, at the start of the flight, when the meteorological sensors equilibrate with the ambient atmospheric conditions and time lags in the temperature (~2.5 s) and humidity (30 or more s) measurements.

The Antarctic atmospheric boundary layer data collected by the SUMO sUAS, described in this paper, are freely available from the United States Antarctic Program Data Center (https://www.usap-dc.org). The data for all flights conducted on the continent (Williams Field, Pegasus ice runway, Tall Tower AWS site and Wright Valley) are available at https://www.usap-dc.org/view/dataset/601054 (Cassano 2017; https://doi.org/10.15784/601054) and data from the PIPERS cruise Ross Sea flights, are available at https://www.usap-dc.org/view/dataset/601191 (Cassano 2019; https://doi.org/10.15784/601191).

The authors also wish to thank Shelley Knuth for her help with flights at Pegasus Runway in September 2012 and Martin Müller and Christian Lindenberg for developing the SUMO sUAS used for this research and providing the training to J.J. Cassano to operate the SUMO and ground station software. We thank the two anonymous referees whose comments helped improve the manuscript.

455

References

Ackley, S.F., Stammerjohn, S., Maksym, T., Smith, M., Cassano, J., Guest, P., Tison, J.-L., Delille, B., Loose, B., Sedwick, P., DePace, L., Roach, L., and Parno, J.: Sea-ice production and air/ice/ocean/biogeochemistry interactions in thee Ross Sea during the PIPERS 2017 autumn field campaign. Annals of Glaciology, doi:10.1017/aog.2020.31, 2020.

460

Båserud, L., Reuder, J., Jonassen, M.O., Bonin, T.A., Chilson, P.B., Jimenez, M.A., and Durand, P.: Potential and limitations in estimating sensible heat flux profiles from consecutive temperature profiling by RPAS, Boundary-Layer Meteorology, 174, 145-177, DOI: 10.1007/s10546- 019-00478-9, 2020.

465

Bonin, T., Chilson, P., Zielke B., and Fedorovich, E.: Observations of the early evening boundary-layer transition using a small unmanned aerial system. Boundary-Layer Meteorology, 146, 119-132, DOI:10,1007/s10546-012-9760-3, 2013.

Cassano, J.J.: Observations of atmospheric boundary layer temperature profiles with a small unmanned aerial vehicle. Antarctic Science, 26, 205-213, doi:10/1017/S0954102013000539, 2014.

470

Cassano, J.: SUMO unmanned aerial system (UAS) atmospheric data, U.S. Antarctic Program (USAP) Data Center. doi:10.15784/601054, 2017.

Cassano, J.: SUMO unmanned aerial system (UAS) atmospheric data, U.S. Antarctic Program (USAP) Data Center. doi:10.15784/601191, 2019.

475

Cassano, J.J., Maslanik, J.A., Zappa, C.J., Gordon, A.L., Cullather, R.I., and Knuth, S.L.: Observations of an Antarctic polynya with unmanned aircraft systems, Eos, 91, 245-246, 2010.

24

Cassano, J.J., Nigro, M.A., and Lazzara, M.A.: Characteristics of the near-surface atmosphere over

480   the Ross Ice Shelf, Antarctica, Journal of Geophysical Research., 121, 3339-3362, doi:10.1002/2015JD024383, 2016a.

Cassano, J.J., Seefeldt, M.W., Palo, S., Knuth, S.L., Bradley, A., Herrman, P.D., Kernebone, P.A., and Logan, N.J.: Observations of the atmosphere and surface state over Terra Nova Bay, Antarctica using unmanned aircraft systems, Earth System Science Data, 8, 115-126,

485   doi:10.5194/essd-115-2016, 2016b.

ENAC (Ecole Nationale de L'Aviation Civile): *Paparrazi user's manual.* http://wiki.paparazziuav.org/w/images/0/0a/Users_manual.pdf, 2008.

Jonassen, M.O., Tisler, P., Altstädter, B., Scholtz, A., Vihma, T., Lampert, A., König-Langlo, G., and Lüpkes, C.: Application of remotely piloted aircraft systems in observing the

490   atmospheric boundary layer over Antarctic sea ice in winter, Polar Research, 34, 25651, DOI:10.3402/polar.v34.25651, 2015.

Katurji, M., Zawar-Reza, P., Zhong, S.: Surface layer response to topographic solar shading in Antarctica's dry valleys, Journal of Geophysical Research., 118, 12332-12344, doi:10.1002/2013JD020530, 2013:

495 King, J.C. and Turner, J.: Antarctic Meteorology and Climatology, Cambridge University Press, Cambridge, United Kingdom, 1997.

Knuth, S.L., Cassano, J.J., Maslanik, J.A., Herrmann, P.D., Kernebone, P.A., Crocker, R.I., and Logan, N.J: Unmanned aircraft system measurements of the atmospheric boundary layer over Terra Nova Bay, Antarctica. Earth System Science Data, 5, 57-69, doi:10.5194/essd-

500   5-57-2013, 2013.

Lawrence, D.A. and Balsley, B.B.: High-resolution atmospheric sensing of multiple atmospheric variables using the DataHawk small airborne measurement system. Journal of Atmospheric and Oceanic Technology, 30, 2352-2366, doi:10.1175/JTECH-D-12-00089.1, 2013.

Mayer, S., Hattenberger, G., Brisset, P., Jonassen, M. and Reuder, J.: A "no-flow-sensor" wind

510   estimation algorithm for unmanned aerial systems. International Journal of Micro Air

Vehicles, 4, 15-30, doi:10.1260/1756-8293.4.1.15, 2012.

Nigro, M.A., Cassano, J.J., Wille, J., Bromwich, D.H., and Lazzara, M.A.: A self-organizing map-

based evaluation of the Antarctic Mesoscale Prediction System using observations from a

30-m instrumented tower on the Ross Ice Shelf, Antarctica. Weather and Forecasting, 32,

515   223-242, DOI:10.1175/WAF-D-16-0084.1, 2017.

Powers, J.G., Manning, K.W., Bromwich, D.H., Cassano, J.J., and Cayette, A.M.: A decade of

Antarctic science support through AMPS. Bulletin of the American Meteorological Society.,

93, 1699-1712, DOI:10.1175/BAMS-D-11-00186.1, 2012.

Reuder, J., Brisset, P., Jonassen, M., Müller, M. and Mayer, S.: The Small Unmanned

520   Meteorological Observer SUMO: A new tool for atmospheric boundary layer research,

Meteorologische Zeitschrift, 18, 2, 141-147, 2009

Reuder, J., Jonassen, M.O., and Olafsson, H.: The Small Unmanned Meteorological Observer

SUMO: Recent developments and applications of a micro-UAS for atmospheric boundary

layer research. Acta Geophysica, 60, 1454-1473, doi:10.2478/s11600-012-0042-8, 2012.

525   Stull, R.B.: An Introduction to Boundary-Layer Meteorology, Kluwer Academic, Dordrecht,

Netherlands, 1988.

Summerhayes, C.P.: International collaboration in Antarctica: The International Polar Years, the

International Geophysical Year, and the Scientific Committee on Antarctic Research, Polar

Record, 44, 321-334, doi:10.1017/S0032247408007468, 2008.

530   Wille, J.D., Bromwich, D.H., Cassano, J.J., Nigro, M.A., Mateling, M.E., and Lazzara, M.A.:

Evaluation of the AMPS boundary layer simulations on the Ross Ice Shelf, Antarctica with

unmanned aircraft observations. Journal of Applied Meteorology and Climatology, 56,

2239-2258, DOI:10.1175/JAMC-D-16-0339.1, 2017.

Deleted: Bull. Amer. Meteor. Soc

Formatted: Font: (Default) Arial, 10 pt
Formatted: Font: (Default) Arial, 10 pt
Formatted: Font: (Default) Arial, 10 pt
Formatted: Font: (Default) Arial, 10 pt
Formatted: Font: (Default) Arial, 10 pt
Formatted: Font: (Default) Arial, 10 pt

Deleted:

Deleted: J. Appl. Meteor. and Clim.

Appendix A

Table A1: UTC date and time (yymmdd HHMM format; yy – year; mm – month; dd – day; HH – hour; MM - minute), location, flight duration (seconds), maximum altitude above ground level (agl) and profile type (SA – stepped ascent; CA – continuous ascent; SD – stepped descent; CD – continuous descent) for all SUMO flights.

Date and time (UTC)	Location	Flight Duration (sec)	Maximum altitude (m agl)	Profile Type
20120114 1810	Williams Field	1817	1002	SA-CD
20120121 1237	Williams Field	1828	1005	SA-CD
20120121 1659	Williams Field	1756	999	SA-CD
20120121 1842	Williams Field	1603	1008	SA-CD
20120128 0022	Williams Field	1453	713	SA-CD
20120128 1254	Williams Field	1497	1013	2 CA-CD
20120128 1641	Williams Field	1175	1025	SA-CD
20120128 1910	Williams Field	2055	1371	SA-CD
20120912 2031	Pegasus Runway	1002	1014	CA-CD
20120915 1947	Pegasus Runway	1730	886	SA-CD
20120915 2103	Pegasus Runway	2145	969	CA-CD
20120915 2230	Pegasus Runway	2448	1015	SA-SD
20120916 0255	Pegasus Runway	2141	776	SA-SD
20120923 2004	Pegasus Runway	1892	510	SA-CD
20140116 0031	Tall Tower	1704	418	SA-CD
20140116 0308	Tall Tower	2250	540	SA-CD
20140116 2336	Tall Tower	1299	526	SA-CD
20140117 0027	Tall Tower	1105	256	CA-CD
20140117 0129	Tall Tower	1423	553	SA-CD
20140117 0310	Tall Tower	1293	654	SA-CD
20140118 2226	Tall Tower	1568	621	SA-CD
20140118 2345	Tall Tower	1405	717	SA-CD
20140119 0119	Tall Tower	1620	802	SA-CD
20140119 0232	Tall Tower	1276	614	SA-CD
20140119 0404	Tall Tower	1213	398	SA-CD
20140120 0824	Tall Tower	1089	151	SA-CD
20140120 1916	Tall Tower	1112	321	SA-CD
20140120 2015	Tall Tower	1419	714	SA-CD
20140120 2308	Tall Tower	1324	599	SA-CD
20140121 0035	Tall Tower	1376	798	SA-CD
20140121 0204	Tall Tower	1321	600	SA-CD
20140121 0333	Tall Tower	1220	514	SA-CD
20140121 0459	Tall Tower	1415	595	SA-CD
20140121 0631	Tall Tower	1166	416	SA-CD
20140121 0802	Tall Tower	1210	400	SA-CD
20140121 0945	Tall Tower	1319	490	SA-CD
20140122 0025	Tall Tower	1203	283	CA-CD
20140122 2111	Tall Tower	1511	687	SA-CD
20140122 2324	Tall Tower	1210	621	SA-CD

27

20140123_0116	Tall Tower	1249	498	SA-CD
20140123_0419	Tall Tower	1445	690	SA-CD
20140123_0620	Tall Tower	1210	502	SA-CD
20140123_2024	Tall Tower	1226	511	SA-CD
20140123_2150	Tall Tower	1462	693	SA-CD
20140123_2318	Tall Tower	1193	610	SA-CD
20140124_0051	Tall Tower	1193	600	SA-CD
20140124_0225	Tall Tower	1320	720	SA-CD
20140124_0351	Tall Tower	1071	403	SA-CD
20140124_0510	Tall Tower	769	196	CA-CD
20140124_0837	Tall Tower	1339	696	SA-CD
20160907_0151	Pegasus Runway	1311	507	SA-SD
20160907_0333	Pegasus Runway	1008	173	SA-CD
20160907_0527	Pegasus Runway	1332	519	SA-SD
20160907_2202	Pegasus Runway	1634	513	SA-SD
20160907_2334	Pegasus Runway	1725	507	SA-SD
20160908_0256	Pegasus Runway	1809	524	SA-SD
20160908_0445	Pegasus Runway	1645	506	SA-SD
20160910_0335	Pegasus Runway	2024	498	SA-SD
20160910_0524	Pegasus Runway	1789	506	SA-SD
20160910_0708	Pegasus Runway	1859	507	SA-SD
20160910_0854	Pegasus Runway	1703	507	SA-SD
20160910_1043	Pegasus Runway	1794	509	SA-SD
20160911_0909	Pegasus Runway	1847	503	SA-SD
20160911_1055	Pegasus Runway	1634	516	SA-SD
20160911_1243	Pegasus Runway	1752	512	SA-SD
20160911_1427	Pegasus Runway	1628	495	SA-SD
20160912_0913	Pegasus Runway	1760	511	SA-SD
20160912_1049	Pegasus Runway	1681	508	SA-SD
20160912_1226	Pegasus Runway	1727	506	SA-SD
20160912_1434	Pegasus Runway	1742	509	SA-SD
20160912_1658	Pegasus Runway	1831	511	SA-SD
20160917_0405	Pegasus Runway	1898	512	SA-SD
20160917_0541	Pegasus Runway	2109	505	SA-SD
20160919_0612	Pegasus Runway	2229	508	SA-SD
20160919_0809	Pegasus Runway	2021	506	SA-SD
20160919_2125	Pegasus Runway	2343	514	SA-SD
20160924_0115	Pegasus Runway	1981	515	SA-SD
20160924_0318	Pegasus Runway	2112	507	SA-SD
20160924_0718	Pegasus Runway	2240	506	SA-SD
20160927_0127	Pegasus Runway	1995	507	SA-SD
20160928_0114	Pegasus Runway	1892	505	SA-SD
20160928_0724	Pegasus Runway	2147	503	SA-SD
20160928_1601	Pegasus Runway	2016	494	SA-SD
20170112_2135	Lake Vanda	1638	797	SA-CD
20170114_2119	Lake Vanda	1797	792	SA-CD
20170115_0325	Lake Vanda	1759	797	SA-CD
20170115_1205	Lake Vanda	1422	784	SA-CD
20170115_1309	Lake Vanda	1642	796	SA-CD
20170116_1123	Lake Vanda	1500	800	SA-CD
20170116_1321	Lake Vanda	1447	813	SA-CD
20170116_1517	Lake Vanda	1442	797	SA-CD
20170116_1559	Lake Vanda	1507	805	SA-CD

20170116_1700	Lake Vanda	1453	795	SA-CD
20170117_1934	Lake Vanda	1482	798	SA-CD
20170117_2041	Lake Vanda	1690	797	SA-CD
20170118_0057	Lake Vanda	1569	801	SA-CD
20170118_0201	Lake Vanda	1496	818	SA-CD
20170425_0434	Ice Station 1	796	89	2 CA-CD
20170425_0550	Ice Station 1	986	194	SA-CD
20170425_0850	Ice Station 1	1522	501	SA-CD
20170426_0234	Ice Station 2	1175	383	SA-CD
20170513_2307	Ice Station 3	918	256	2 CA-CD
20170514_0327	Ice Station 3	952	398	SA-CD
20170514_0912	Ice Station 3	977	405	SA-CD
20170527_0352	Ice Station 7	1467	297	SA-CD
20170527_0444	Ice Station 7	1383	303	SA-CD
20170527_2335	Ice Station 8	1279	599	SA-CD
20170528_0152	Ice Station 8	414	119	2 CA-CD
20170529_0836	Ice Station 9	647	216	SA-CD
20170529_1050	Ice Station 9	1712	902	SA-CD
20170529_1227	Ice Station 9	1460	897	SA-CD
20170531_0206	Ice Station 10	1651	907	SA-CD
20170531_0511	Ice Station 10	1919	908	SA-CD
20170531_2046	Ice Station 11	459	154	SA-CD
20170602_0314	Ice Station 12	1758	898	SA-CD
20170602_0618	Ice Station 12	1714	808	SA-CD

545

555   Table A2. Post-processed SUMO data files and data archived in each type of post-processed file.

Post-processed SUMO data file[*]	Variables stored in file
yy_mm_dd__HH_MM_SS_SD.txt	UTC year, month, day, hour, minute, second
yy_mm_dd__HH_MM_SS_SD_interpolation.txt	Elapsed time since SUMO power on (sec)
	Easting, northing, altitude (m)
	GPS speed (m s^{-1})
	Relative humidity from SHT sensor (%)
	Temperature from SHT and Pt sensors (deg C)
	Pressure from VTI sensor (mb)
	Downward facing infrared temperature (deg C)
	Original observation flag
yy_mm_dd__HH_MM_SS_SD_const_alt.txt	Count – sequential counter identifying each constant altitude orbit
	UTC year, month, day, hour, min, sec
	Time (sec)
	Altitude (m)
	Pressure (mb)
	Temperature (SHT, Pt and IR) (deg C)
	RH (%)
	Wind speed (m s^{-1})
	Wind direction (deg) (two estimates)
	Constant altitude orbit time start and end (sec)
	Total time for constant altitude orbit (sec)
	SUMO heading at start and end of constant altitude orbit (deg)
	Summed change in heading over orbit (deg)
	Start and end altitude for constant altitude orbit (m)
	GPS minimum and maximum speed on constant altitude orbit (m s^{-1})
	Heading at mimimum and maximum GPS speed (deg)
yy_mm_dd__HH_MM_SS_SD_vert_avg.txt	Bin altitude (m)
	For each of the following variables the bin average, standard deviation and number of observations used to calculate the bin average are reported for all observations

	during the flight and for all ascent-only and all descent-only observations.
	Altitude (m)
	RH (%)
	Temperature (SHT, Pt and IR) (deg C)
	Pressure (mb)

* _SD portion of filename is omitted if data came from telemetry data stream rather than SD data stream.

560